Journal of Visualization, Vol. 10, No. 2 (2007)237-244

Regular Paper

Behavior of Underexpanded Plasma Jet in Strong Magnetic Field

Ono, N.*[1], Otomo, Y.*[2] and Koike, K.*[1]

*1 Department of Mechanical Engineering and Intelligent Systems, Tohoku Gakuin University, 1-13-1 Chuo, Tagajo, Miyagi 985-8537, Japan.
E-mail: norifumi@tjcc.tohoku-gakuin.ac.jp / koike@tjcc.tohoku-gakuin.ac.jp
*2 Graduate School, Tohoku Gakuin University, 1-13-1 Chuo, Tagajo, Miyagi 985-8537, Japan.

Received 14 October 2006
Revised 16 December 2006

Abstract : A visual study of underexpanded plasma jet was conducted to reveal the detailed behavior in the strong magnetic field. The images of the jet were taken by a digital single-lens reflex camera through viewing windows. The distribution of optical intensity obtained from the raw data was compared to that of the typical emission line intensity. The profile of the optical intensity agrees well with that of the emission intensity. It is illustrated that the typical structure of underexpanded jet such as Mach disk is also affected obviously by the magnetic field. The radial distribution of number density was determined by using the image analysis based on the Abel-inversion. The converted data clarify the jet behavior that is hidden on the ordinary observation. The density obtained from numerical analysis for a simple gas was also compared with the number density. It is confirmed from the comparison with numerical results that the radial profile of number density can be utilized for understanding the plasma jet behavior under the strong magnetic field.

Keywords : Plasma, Jet, Functional fluid, Magnetic field, Image analysis, Abel-inversion.

1. Introduction

Recently, applications using plasma jet have been developed actively in various fields. In these applications it is desirable to control the plasma jet precisely. Plasma jets are also known as the functional fluid flow in the magnetic field (Nishiyama et al., 1995). It is expected that the flow characteristics could be improved by the applied strong magnetic field and that the functional enhancement of plasma jet under the strong field will be useful for developing the space propulsion system in the future and the material processing technology. It is, therefore, important to investigate the jet behavior under such strong field as imposed by a superconducting magnet. However, the behavior of plasma jets under the strong field has not sufficiently been clarified.

On the other hand, visual studies of the supersonic flow with shock waves have been conducted to reveal the characteristics (e.g., Sun et al., 2003). In the visualization of shock waves the method using the electric discharge (e.g., Viren et al., 2005) has been used frequently. Also, the behavior of plasma jet can be observed directly by using its luminosity (e.g., Yano et al., 2000).

From these points of view, experimental studies have been carried out to examine the effect of the strong magnetic field on argon plasma jets (e.g., Koike et al., 2004). Emission measurement, in these studies, was performed at lateral positions from the center to the outer edge of the jet to determine the excitation temperature distribution. In the present visual study the images of plasma

jet in a vacuum chamber were taken by a digital single-lens reflex camera with high spatial resolution through viewing windows. The distribution of optical intensity was obtained by the image analysis using the software that was developed to study the plasma jet behavior. The lateral distribution of the optical intensity was compared to that of the emission line intensity. The radial distribution of number density was determined by using the image analysis based on the Abel-inversion. It was also compared with the density distribution obtained from numerical analysis for a simple gas.

2. Experimental and Numerical Method

2.1 Experimental Setup and Procedures

Argon plasma jet was generated in a vacuum chamber with a vacuum pump system. The jet is assumed to be an axisymmetric flow without swirl in the present study. The axisymmetric coordinate system used here is indicated in Fig. 1. The dimensions of supersonic nozzle constructed by anode wall are also shown in this figure. The nozzle exit diameter d_e is 7.5 mm and the throat diameter is 5 mm. Thus, the divergent ratio (exit / throat area) is 2.25. The background chamber pressure p_b is maintained at 378 ± 41 Pa in the case of the mass flow rate of the jet $\dot{m} = 1.20 \pm 0.02$ g/s. The flow from nozzle exit is a typical underexpanded jet. The inherent behavior of the jet such as Mach disk and reflected shock was also illustrated schematically in this figure. The origin is located on intersection of the nozzle exit and center axis. The flow direction indicated by the arrow is defined as x–coordinate, and z–axis is perpendicular to x–axis. The magnet composed of a pair of superconducting coils imposes the magnetic field to the jet. The magnetic field distribution along the center axis is shown in the right bottom part of this figure in the case of the magnetic flux density at the midpoint B_c = 1.5 T. The plasma torch is movable along the centerline of magnet bore. The distance along the centerline between the torch exit plane and the focused point of optical probe, L, was fixed to be 400 mm. It also was set to be 350 mm to compare the effect of magnetic field configuration on the jet.

The images of plasma jet were taken by the digital single-lens reflex camera with high spatial resolution through viewing windows. The jet from the plasma torch to the entrance of magnet bore (cf. middle part in Fig. 1) was observed by a window named ‘upstream window’. The jet behavior between the coils (cf. right side in Fig. 1) can be seen through a window named ‘center window’ at opposite side of the optical probe. Two cameras (Nikon D2x) were employed to obtain the image through the windows. The spatial resolutions of image are about 0.1 mm/pixel for the upstream and 0.075 mm/pixel for the center window. The selected image format in the present analysis is ‘raw data format’, which records signals directly from the charge-coupled device (CCD) in the camera. The resolution of raw data is 12bit, or 4096/pixel. The image analysis software was also developed to study the plasma jet behavior. The focal point of the optical probe for spectroscopic diagnostics was placed at the middle between both coils. The emission measurement using a traverse assembly of optical probe was performed at lateral positions from the center to the outer edge of the jet in 1 mm

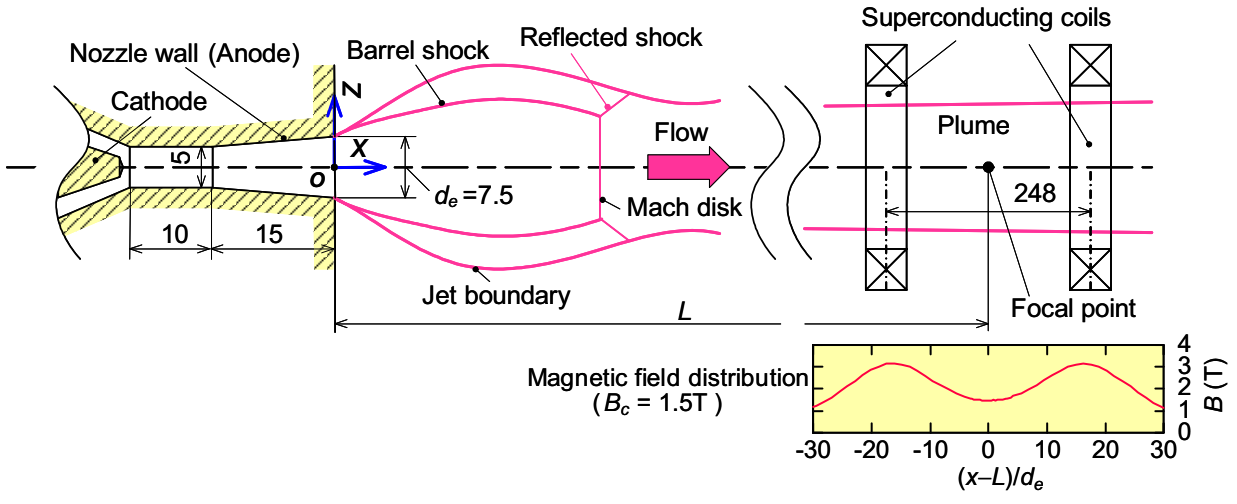

Fig. 1. Axisymmetric coordinate system and schematic view of typical structure for underexpanded jet.

intervals. The measurable region is restricted within the lateral positions at the middle between both coils.

2.2 Numerical Analysis

The numerical calculation based on the Chakravarthy-Osher TVD (Total Variation Diminishing) scheme (Chakravarthy and Osher, 1985) was conducted to predict the fundamental behavior of the underexpanded jet in the experiment. The governing equations are the Navier-Stokes equations for laminar flow. The axisymmetric flow of a simple gas is assumed to be a compressible fluid. The nozzle dimension is similar to that of experimental apparatus.

3. Results and Discussion

3.1 Comparison of Optical Intensity with Emission Line Intensity

Examples of the jet images observed through the center window for L = 400 mm and for L = 350 mm are shown in Fig. 2. The supplied current to plasma torch i_s is 125 A and the magnetic flux density B_c is 1.0 T. The photographs are inverted so that the flow direction is left-to-right. The brightness for L = 350 mm is higher than that for L = 400 mm. It is the reason the electrical conductivity of the plasma jet is high for L = 350 mm because of the short distance from the torch exit to observed point. Figure 3 plots the typical emission line intensity (wavelength λ = 603.21 nm) under the same conditions in Fig. 2. The data described here were obtained by scanning the monochromator from 564 to 623 nm in wavelength. The emission line intensity is normalized by the maximum value for L = 400 mm. The lateral distribution of optical intensity obtained from the raw data is also indicated in this figure. The optical intensity is normalized like the emission intensity. The relationship between the emission intensity I_p and the optical intensity I_v is estimated as the following expression.

$$I_v \propto \int I_p \, d\lambda \tag{1}$$

On the other hand, it is inferred that the integrated emission intensity over all range of wavelength is almost proportional to the dominant line intensity. As a result, the relationship between optical and emission intensity is written simply by Eq. (2).

$$\frac{I_v}{I_{v\max}} = \frac{I_p}{I_{p\max}} \tag{2}$$

The raw data was obtained when the position of movable probe is just on the center axis. In contrast, it takes approximately ten minutes to traverse the probe for the emission distribution measurement. Although the measuring time scale is different, it is indicated that the distribution of optical intensity is in good agreement with that of the emission. The analysis using the optical intensity can be utilized for a simple diagnosis of the jet because the raw date can be quickly obtained over the wide area in the jet.

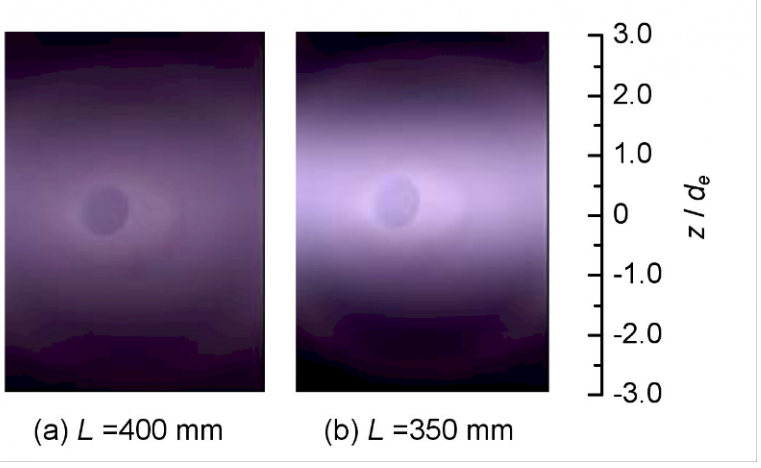

Fig. 2. Plasma jet observed through the center window (i_s = 125 A, B_c = 1.0 T).

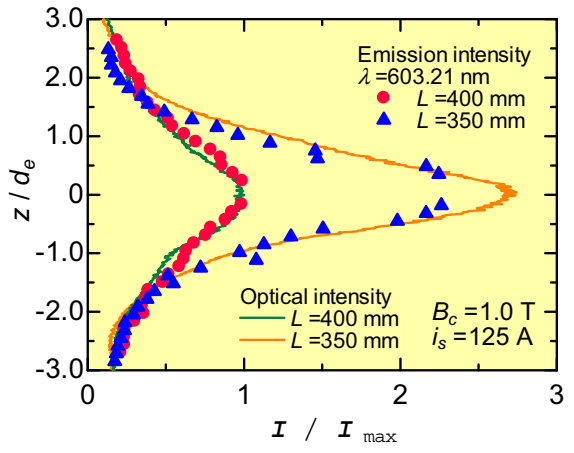

Fig. 3. Comparison between optical and emission line intensity.

3.2 Flow Behavior of Underexpanded Plasma Jet

Figure 4 shows plasma jet observed through the upstream window for L=400 mm(x/d_e = 0 – 16, z/d_e = 0 – 4). It is clearly indicated that the jet has typical characteristics of strong axisymmetric underexpanded jet such as Mach disk and barrel shock. The high brightness region appears downstream of the Mach disk and regenerates further downstream of the disk. It is found that the intensity in the high brightness region increases with the application of magnetic field. It has been inferred from the previous study (Ono et al., 2004) that the Mach disk location is not significantly affected by the field. Figure 5 also shows the jet image for L = 350 mm. The image length for L = 350 mm is shorter (x/d_e = 0 – 12) than that for L = 400 mm due to the location of the magnet. The image shows similar trend to Fig.4 for L = 400 mm. It is found that the brightness for L = 350 mm is higher in the applied magnetic field than that for L = 400 mm because of the same reason as Fig. 2.

The raw data is unsuitable for displaying the images directly because the contrast is much low. Thus, the color mapping, which is frequently used in the contour plots, as shown in Fig. 6 is introduced to indicate the distribution of optical intensity. Figures 7 and 8 indicate the distribution of optical intensity for L = 400 mm and for L = 350 mm, respectively. The color mapping represents the variation of the optical intensity clearer than that of the ordinary color intensity as shown in Figs. 4 and 5.

The relationship between typical emission line intensity I_p and the number density of the upper excited level n_j is represented by Eq. (3) (Ono et al., 2005).

$$\frac{I_p}{I_{p\max}} = \frac{n_j}{n_{j\max}} \tag{3}$$

Thus, from Eqs. (2) and (3), the ratio of I_v corresponds to that of number density n_j. Commonly, the radial distribution of density is calculated in the numerical analysis of the axisymmetric flow. To compare with the numerical data, the density distributions have to be converted to the values in the radial direction. Therefore, the Abel-inversion that is frequently used to determine the radial temperature distribution is introduced for the conversion of the images. The expression for Abel-inversion is as follows.

$$\varepsilon(r) = -\frac{1}{\pi}\int_r^R \frac{\dfrac{dI(z)}{dz}}{\sqrt{z^2 - r^2}}dz \tag{4}$$

Here, r and R denote radial coordinate and radius of the jet, respectively. ε is the emission intensity coefficient. The ratio of the emission coefficient to the maximum value also corresponds to the ratio of number density to the maximum one. Thus, in the following descriptions, the number density in the lateral and the radial distribution is written briefly as $n/n_{\max}$.

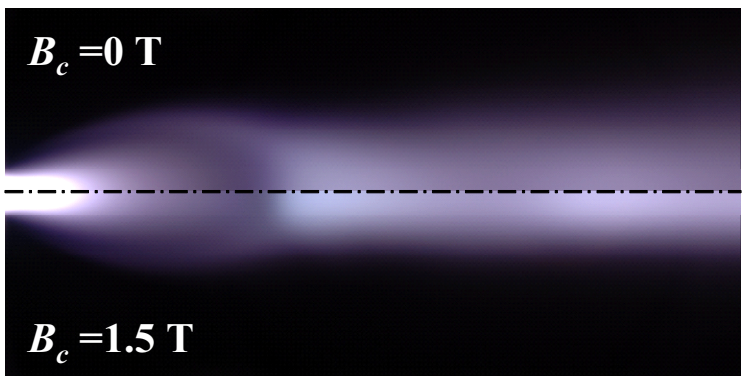

Fig. 4. Plasma jet observed through the upstream window for L = 400 mm.

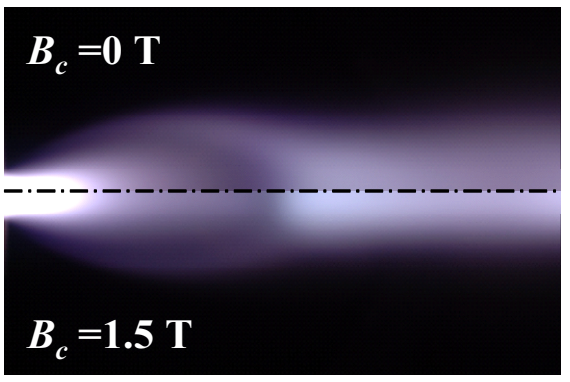

Fig. 5. Plasma jet observed through the upstream window for L = 350 mm.

Fig. 6. Color mapping.

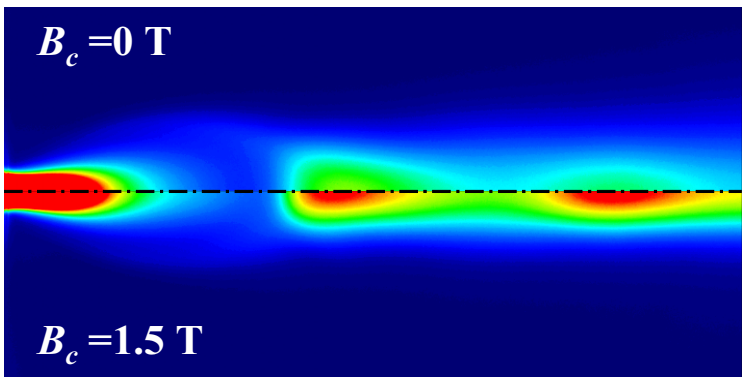

Fig. 7. Optical intensity of plasma jet for L = 400 mm.

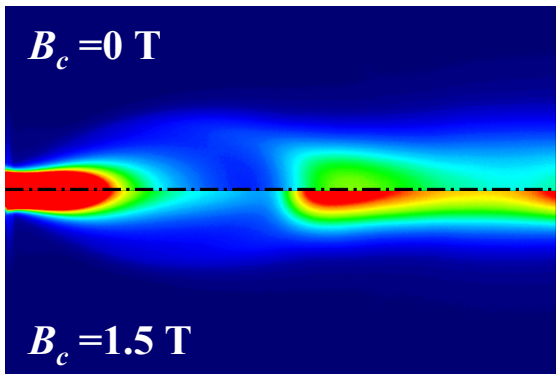

Fig. 8. Optical intensity of plasma jet for L = 350 mm.

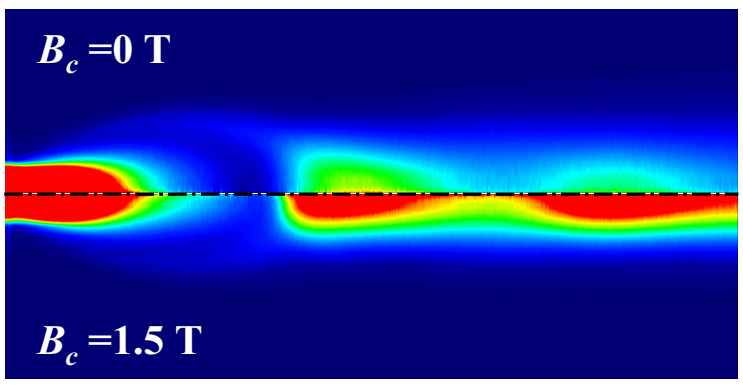

Fig. 9. Modified radial distribution of number density of plasma jet for L = 400 mm.

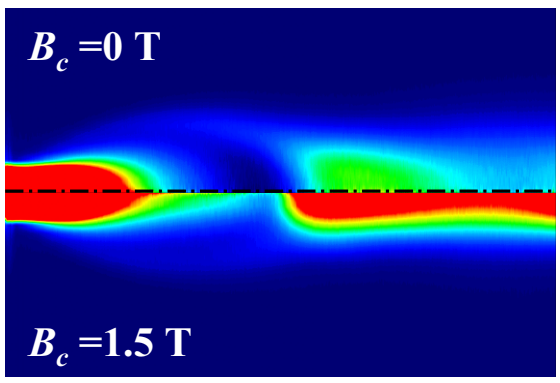

Fig. 10. Modified radial distribution of number density of plasma jet for L = 350 mm.

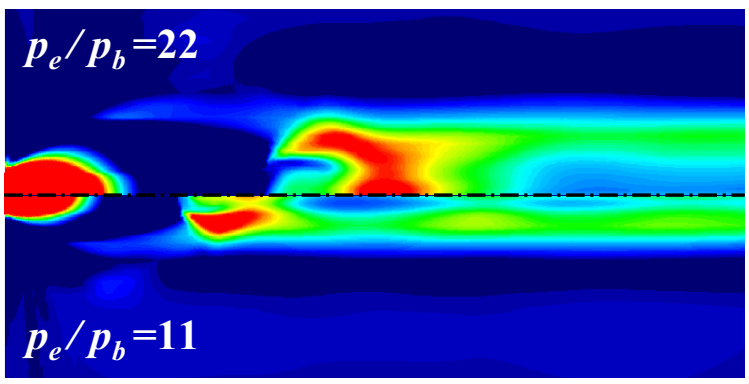

Fig. 11. Predicted radial distribution of density for underexpanded jet (Simple gas model).

Figures 9 and 10 show modified radial distribution of number density for the plasma jet for L = 400 mm and for L = 350 mm, respectively. Naturally, the lower the intensity near center axis for lateral distribution is, the lower the part of the image at the present location for radial distribution is converted. In contrast, the higher the intensity at the position away from the center becomes, the higher the part of the image is transformed. Therefore, the density, upstream of the Mach disk, becomes lower than that before modification. The density around the reflected shock is high. Then, the density near center axis is enhanced due to the compression with the application of the magnetic field.

The density for the underexpanded jet is also obtained from the numerical analysis with the assumption of a simple gas. Examples of the radial density distribution are presented in Fig. 11. In

this figure, p_e / p_b denotes the ratio of the pressure at the nozzle exit to the background pressure. Generally, the outer contour of the jet increases with an increase in the pressure ratio (e.g., Cumber et al., 1995). It is also confirmed that the density upstream of the Mach disk is low and that the density around the reflected shock is high. Thus, it is thought that the images as shown in Figs. 9 and 10 express the distribution of number density approximately. From the images of radial distribution of number density, it is possible to consider simply the behavior of plasma jet in the radial direction.

3.3 Number Density Distribution of Plasma Jet

Figure 12 shows the distributions of the number density at streamwise locations under various conditions. The radial and lateral distributions show in the top and bottom of each figure, respectively. The number density is normalized by the maximum value at $x / d_e = 8$. The Mach disk appears around $x / d_e = 6$ under all conditions in the present data (cf. Figs. 9 and 10). The density clearly increases downstream of the disk with the applied magnetic field. It is nearly uniform around Mach disk without the field. It enhances toward the center axis with the application of strong magnetic field. In the previous visual study (Ono et al., 2004), it has been considered that the area upstream of the Mach disk is hardly affected by the field. However, it is confirmed from the analysis using the raw data that the density distribution upstream of the disk changes by the field.

Figures 13 and 14 also indicate the lateral and radial distributions of the number density near the Mack disk for $L = 400$ mm. The number density is normalized by the maximum value at $x / d_e = 8$ as same as Fig. 12 although the distribution at $x / d_e = 8$ is not included in these figures. The increase of density downstream of the reflected shock is explicitly detected in the radial distribution without

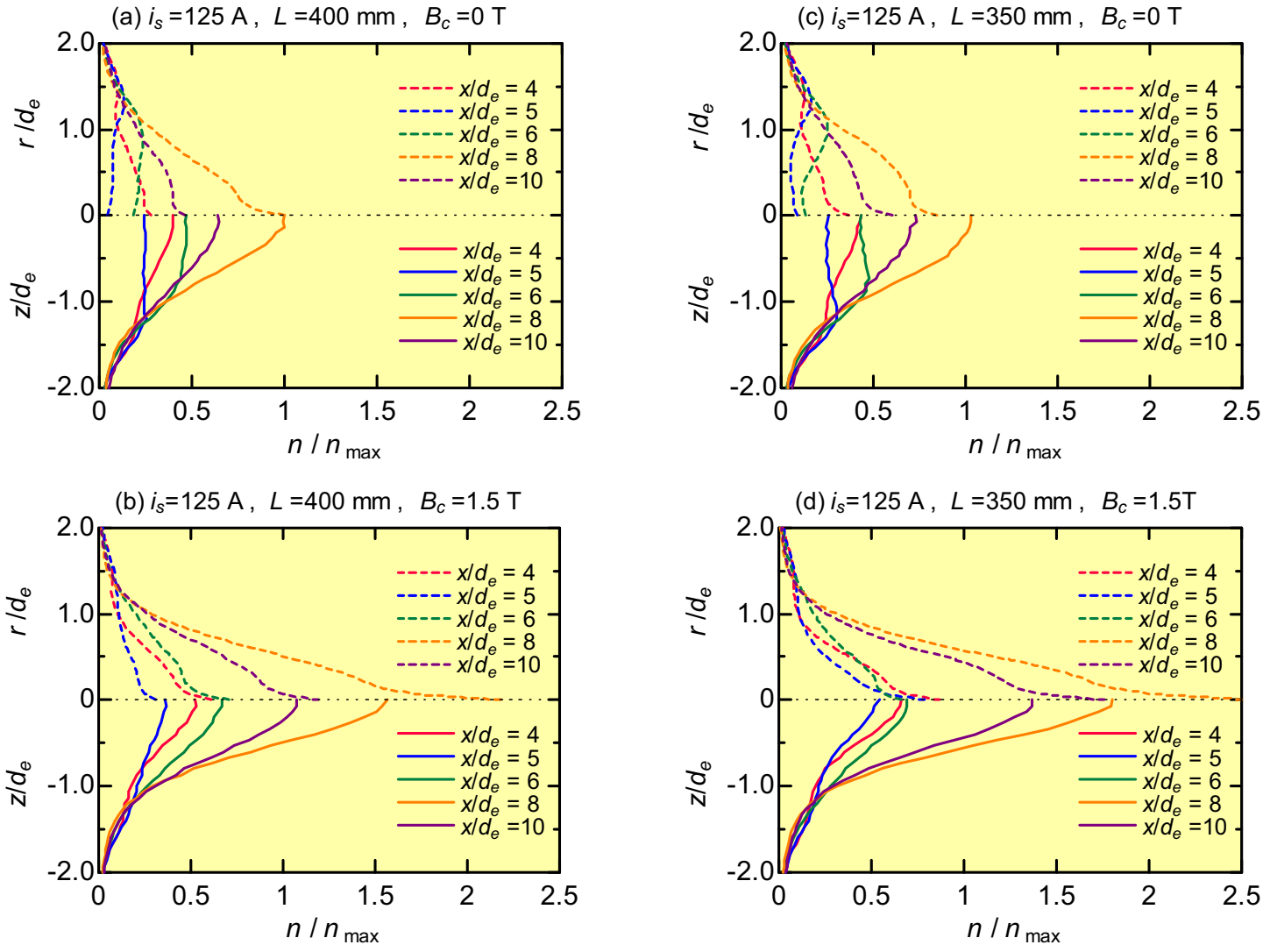

Fig. 12. Radial and lateral distribution of number density.

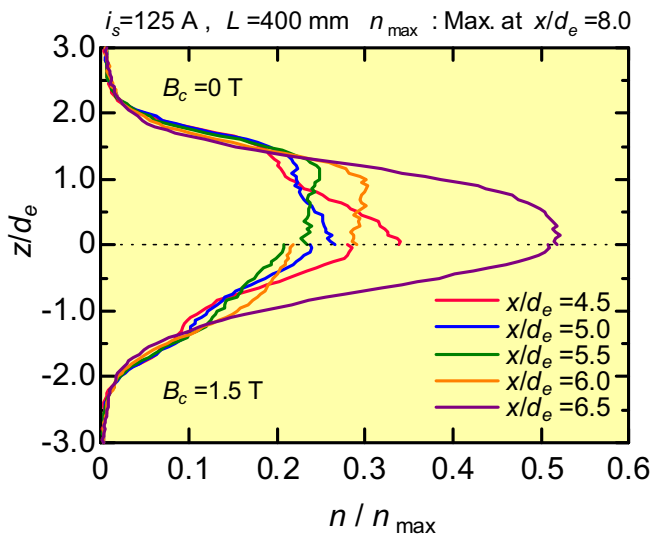

Fig. 13. Lateral distribution of number density near the Mach disk.

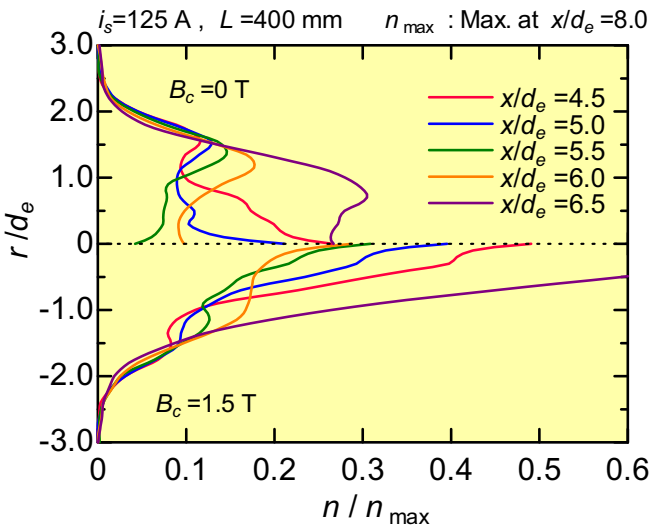

Fig. 14. Radial distribution of number density near the Mach disk.

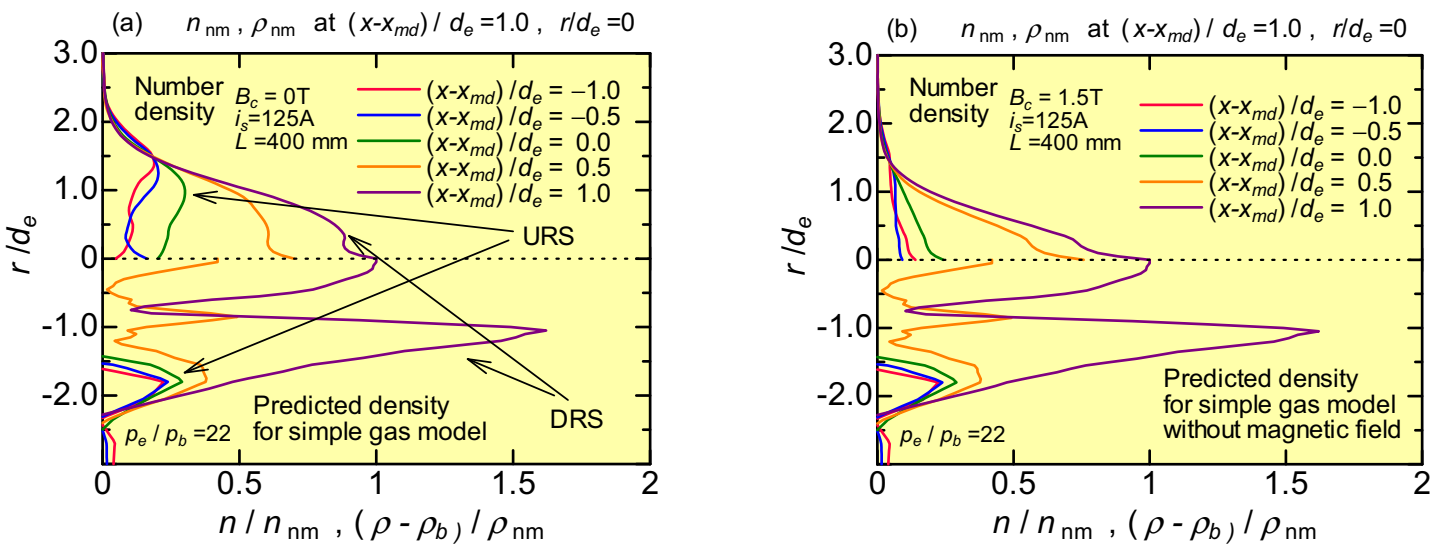

Fig. 15. Comparison between number density and predicted density near the Mach disk.

the field. It is also slightly observed in the case of the application of the field. Because the jet behavior is hidden on the ordinary observation, it is valuable to consider with the data obtained from the Abel-inversion.

The comparison of the radial distributions near the Mach disk between the number density obtained from the raw data and the predicted density calculated from the numerical analysis is represented in Fig. 15. The number densities in left (a) and right (b) figures denote the data with and without magnetic field, respectively. In this figure, x_{md} denotes the Mach disk position and ρ_b is the background density. The number density and the predicted density are normalized by the value [n_{nm}, ρ_{nm}] at $(x-x_{md}) / d_e = 1.0$ and $r / d_e = 0$. 'URS' means the location upstream of the reflected shock and 'DRS' denotes the position downstream of the reflected shock. It is shown that the density downstream of the reflected shock rises due to the shock effect. From the comparison with numerical data, it is confirmed that the number density based on the raw data can display qualitatively the behavior of the jet in the radial direction.

4. Conclusion

A visual study of underexpanded plasma jet is carried out to clarify the detailed behavior in the strong magnetic field. The results obtained here are summarized as follows.

1. The lateral distribution of optical intensity based on the raw data taken by the digital camera agrees well with that of emission line intensity. The optical intensity can be utilized for a simple diagnosis of the plasma jet.

2. It is confirmed that the density around the center axis becomes much higher with the applied magnetic field than that without the field since the jet is contracted by the strong field.

3. The modified radial distributions of number density were drawn by using the Abel-inversion. They show qualitatively good agreement with those of the predicted density for a simple gas. It is considered that the obtained distributions of number density fairly express the behavior of the plasma jet in the radial direction.

4. The increase of density downstream of the reflected shock is explicitly detected in the radial distribution without the field. The jet behavior, hidden on the ordinary observation, is revealed from the converted data with the Abel-inversion.

References

Chakravarthy, S. and Osher, S., A New Class of High Accuracy TVD Schemes for Hyperbolic Conservation Laws, AIAA Paper, No. 85-0363 (1985).

Cumber, P. S., Fairweather, M., Falle, S. A. E. G. and Giddings, J. R., Predictions of the Structure of Turbulent, Highly Underexpanded Jets, Transactions of the ASME, Journal of Fluids Engineering, 117 (1995), 599-604.

Koike, K., Ono, N., Watanabe, Y. and Musha, K., Measurement on the Excitation Temperature of Argon Plasma Jet under Strong Magnetic Field, Vacuum, 73 (2004), 353-358

Nishiyama, H., Sato, T., Veefkind, A. and Kamiyama, S., Functional Enhancement of a Nonequilibrium Plasma Jet by Seeding in the Applied Magnetic Field, Heat and Mass Transfer, 30 (1995), 291-296.

Ono, N., Musha, K. and Koike, K., Control of Plasma Jet Using Strong Magnetic Field, JSME International Journal, Series B, 48-3 (2005), 411-416.

Ono, N., Musha, K. and Koike, K., Visualization of Plasma Jet under Strong Magnetic Field, 11th International Symposium on Flow Visualization, University of Notre Dame (Notre Dame, Indiana, USA), (2004), 9 pages, CD-ROM.

Sun, L. Q., Sugiyama, H., Mizobata, K. and Fukuda, K., Numerical and Experimental Investigations on the Mach 2 Pseudo-Shock Wave in a Square Duct, Journal of Visualization, 6-4 (2003), 363-370.

Viren, M., Jagadeesh, G., Reddy, K. P. J., Sun, M. and Takayama, K., Visualization of Shock Waves around Hypersonic Spiked Blunt Cones Using Electric Discharge, Journal of Visualization, 8-1 (2005), 65-72.

Yano, R., Contini, V., Plönjes, E., Palm, P., Merriman, S., Aithal, S., Adamovich, I., Lempert, W., Subramaniam, V. and Rich, J. W., Supersonic Nonequilibrium Plasma Wind-Tunnel Measurements of Shock Modification and Flow Visualization, AIAA JOURNAL, 38-10 (2000), 1879-1888.

Author Profile

Norifumi Ono: He received his M. Sc. (Eng.) degree in Mechanical Engineering in 1991 from Tohoku Gakuin University and his Ph.D. in Mechanical Engineering in 1995 from the same university. He worked in Department of Chemical Energy Engineering, Yokosuka Research Laboratory, Central Research Institute of Electric Power Industry as a visiting researcher in 1995. He then became a Part-time Lecturer of Tohoku Gakuin University in 1997, and currently is an associate professor. His research interests are analysis of plasma jet characteristics, computational fluid simulation and control of flow behavior.

Yasuhumi Otomo: He received his B. Sc. (Eng.) degree in mechanical engineering from Tohoku Gakuin University in 2005. He is currently a graduate student in the Course of Mechanical Engineering, Division of Engineering, Graduate School of Tohoku Gakuin University. His current research interests are focused on improvement of optical techniques for plasma emission measurements and quantitative evaluation on effects of strong magnetic field on plasma jet.

Kazuo Koike: He received his M. Sc. (Eng.) in Mechanical Engineering II in 1973 from Tohoku University. He also received his Ph.D. in Mechanical Engineering II in 1976 from Tohoku University. After completion his Ph.D. program, he has been a faculty member of Institute of High Speed Mechanics, Tohoku University (1976-1988). He then became an associate professor of Tohoku Gakuin University in 1988, and currently is a Professor. His research interests are flow phenomena of functional fluid in strong magnetic field, control of plasma jet using strong magnetic field, and utilization of optical emission spectroscopy and image analysis for plasma diagnostics.